1 A PROJEKT TÉMÁJA

Kutatási területem nagyintenzitású, femtoszekundumos lézerimpulzusokkal gerjesztett nemlineáris folyamatok vizsgálata, melyek attoszekundumos impulzusok keltését teszik lehetővé. Az előállított attoszekundumos impulzusok hossza hasonló a hidrogén atom elektronjának klasszikus keringési idejéhez, így az „attofizika" új tématerületében lehetőség nyílik anyagi elektron-dinamikai folyamatok tanulmányozására eddig ismeretlen időbeli felbontásban.

Ennek a kutatási témának különös jelentőséget biztosít az, hogy egy európai kutatási nagyberendezés (ELI – Extreme Light Infrastructure) létrehozására irányuló program keretében Szegeden épül majd a világ élvonalába tartozó lézerrendszer, melynek fő profilja az attoszekundumos jelenségek vizsgálata lesz.

Manapság kereskedelmi forgalomban kapható femtoszekundumos (1 fs = 10^{-15} s) impulzusokat szolgáltató lézerek alkalmazásával 100-1000-szer rövidebb, attoszekundumos (1 as = 10^{-18} s) impulzusokat lehet létrehozni [G. Farkas, C. Tóth, Phys. Lett. A **168**, 447 (1992)., F. Krausz, M. Ivanov Rev. Mod. Phys. **81**, 163 (2009)]. Rövid fényimpulzusok létrehozása két szempontból is különös jelentőséggel bír. Egyrészt egy impulzus energiáját minél rövidebb időtartamra szorítjuk össze, annál nagyobb csúcs-teljesítményt és erősebb elektromos teret lehet elérni, ami újabb és újabb fény-anyag hatások tanulmányozását teszi lehetővé (meg kell jegyeznem, hogy a jelenleg femtoszekundumos lézerrel elérhető intenzitást a harmonikus generálás alacsony hatásfoka miatt még nem sikerült megközelíteni attoszekundumos impulzusokkal – de a tudományterület fejlődésével ez is elérhetővé válhat). Az impulzusok rövidülésének másik jelentősége abban rejlik, hogy pumpa-próba vizsgálatokban a rendelkezésre álló impulzusok hossza szabja meg gyors folyamatok vizsgálatának időbeli felbontását.

Attoszekundumos impulzusok létrejöttének feltétele, hogy széles spektrumú, koherens sugárzást hozzunk létre az XUV – röntgen tartományban. A spektrumnak olyan nagy tartományt kell átölelnie, hogy nem létezik olyan lézer-anyag, mely ebben a sávszélességben erősíteni tudna, ezért attoszekundumos lézer nem létezhet. Ugyanakkor nemlineáris folyamatok révén (mint például a magas-harmonikus keltés) lehetséges femtoszekundumos lézerimpulzusokat magasabb frekvenciájú spektrális tartományba konvertálni, megteremtve az attoszekundumos impulzusok szintetizálásának lehetőségét. A konverzió révén a magas rendű harmonikusokra átörökítődnek a keltő lézerimpulzustól kedvező optikai tulajdonságai (ultrarövid impulzushossz, magas fotonenergia, irányítottság, nagy fényesség, magas térbeli és időbeli koherencia).

Az elmúlt év kutatási eredményeit négy tématerület köré csoportosítottam:

1. Attoszekundumos impulzusok alakformálása (XAC)
2. Attoszekundumos impulzus-sorozat nem-adiabatikus leírása (gázban keltett harmonikusok)
3. Magasharmonikus keltés plazma felszínen
4. Attoszekundumos impulzusok keltése THz-es tér jelenlétében

2 A MUNKA RÉSZLETES TARTALMI LEÍRÁSA.

2.1 Attoszekundumos impulzusok alakformálása (XAC)

Az attoszekundumos impulzusok egy új spektrális tartomány (XUV – röntgen) meghódításával új mérési, manipulálási eljárásokat igényelnek, hogy a femtoszekundumos tartományban közismert rugalmas alakformálás, diagnosztika elérhető legyen. Az attoszekundumos impulzusok keltésének fizika folyamata magában rejti a keltett impulzusok fázismodulációjának tényét. Egy korábbi publikációban kimutattuk, hogy vékony fém szűrő alkalmas lehet az attoszekundumos impulzusok fázisát kedvezően változtatni, és az impulzusok akár harmad hosszúságra is összenyomhatók [R. López-Martens, *et al.,* Physical Review Letters **94**, 033001 (2005)]. Anyagi diszperzió használatának nagy hátránya, hogy a szűrő csak az adott anyag abszorpciós sávja közelében rendelkezik negatív csoport-késleltetés diszperzióval, vagyis nagyon korlátozott a módszer alkalmazhatósága.

Impulzus kompresszióra, illetve alakformálásra egy másik módszert javasolunk [L. Poletto, P. Villoresi, Appl. Opt. **45**, 34 (2006) alapján], mely súrlódó beesési elrendezésben alkalmazott rácsok kúpos diffrakcióján alapul.

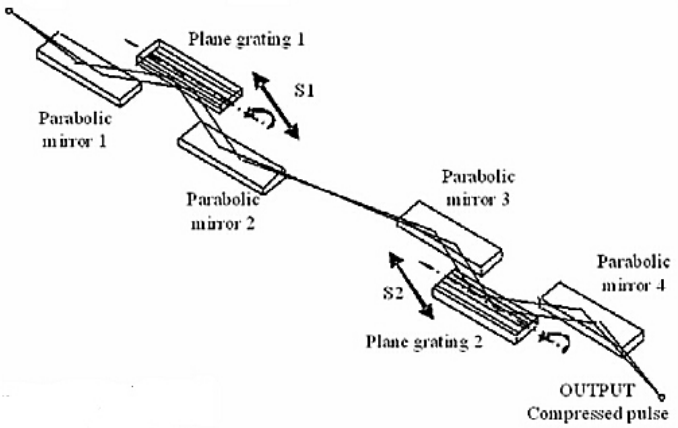

Ez a módszer sokkal rugalmasabb, mint az előzőleg említett anyagi diszperzió és lehetőség van finom, *in situ* hangolásra is. A tervezett kompresszor két rácsból áll, és az XUV tartományban negatív diszperzióval, és közel állandó átvitellel rendelkezik. Széles spektrális tartományban alkalmazható. Az elképzelést numerikus szimulációk segítségével teszteltük a University of Padova kutatócsoportjával együttműködésben.

Vizsgálataink azt mutatták, hogy még abban az esetben is, amikor a lézerimpulzus tulajdonságait (intenzitás) úgy választjuk meg, hogy egy adott fém anyagi diszperziójához jól illeszkedjen a generált spektrum, a rácsos kompresszorral sokkal jobb eredményt értünk el, mind a kompresszió tekintetében, mind az átengedett energia tekintetében.

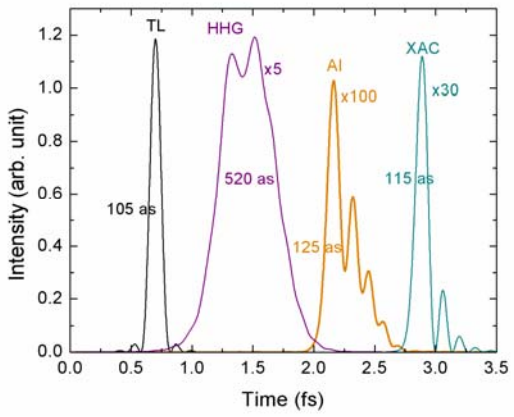

E témában elért eredményeinket három alkalommal mutattuk be nemzetközi konferencián:

R. A. Ineschi, K. Varjú, F. Frassetto, L. Poletto and P. Villoresi: *Design of an adaptive compressor and pulse-shaper for attosecond XUV pulses*, CG.P.9-MON at **CLEO/Europe-EQEC 2009**, Munich, June 14-19

L. Poletto, F. Frassetto, R.A. Ineschi, P. Villoresi, K. Varjú: *Design of an adaptive compression for attosecond XUV pulses*, pp. 136-138 in Proc. **Ultrafast Optics VII, High Field Short Wavelength XIII**, Arcachon, Aug 31-Sep 4, 2009

K Varjú, M Mero, F Frassetto, L Poletto and P Villoresi: *Compression methods for XUV attosecond pulses*, p. 138 (Poster 32) in Book of Abstracts **Light at Extreme Intensities LEI'09** Oct 16-21, Brasov, 2009

A kutatás nyomán egy kézirat is készült, melyet utolsó javítások után rövidesen be fogunk küldeni egy referált folyóirathoz (csatolva):

Katalin Varjú, Roberto Antonio Ineschi, Mark Mero, Fabio Frassetto, Luca Poletto and Paolo Villoresi: *Compression methods for XUV attosecond pulses*

2.2 Attoszekundumos impulzus-sorozat nem-adiabatikus leírása (gázban keltett harmonikusok)

A magas harmonikus keltés folyamatának alapja a lézer elektromégneses terében levő atom optikai ionizációja, az elektronok lézer-térbeli mozgása. Ennek leírását az időfüggő Schrödinger-egyenlet megoldásaként adódó elektron hullámfüggvény adja. Ez a számítás már egyszerű atomok esetén is igen idő igényes, és az eredmények értelmezése nélkülözi a fizikai, intuitiv jelleget. A magas harmonikus jelenség értelmezéséhez rendelkezésre áll egy félklasszikus modell [M. Lewenstein, *et al.*, Phys Rev A **52**, 4747 (1995)], mely a nyeregpont-közelítés alkalmazásával gyorsan eredményhez vezet és alkalmazásával nyert eredményeim a folyamatok alapvető tulajdonságainak megértéséhez segítettek hozzá [K. Varjú, *et al.,* Journal of Modern Optics **52**, 379 (2005), K. Varjú, *et al.,* Phys Rev Lett **95**, 243901 (2005)]. Korábbi munkáimban csak a sugárzás fázisát vizsgáltam, és csak adiabatikus (lassan változó keltő impulzus) esetben. Ezt a modellt fejlesztettem a sugárzás spektrális intenzitásának és a néhány-ciklusú keltő lézerimpulzus esetében fellépő nem-adiabatikus jellegek vizsgálhatóságának érdekében.

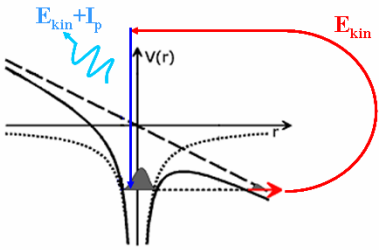

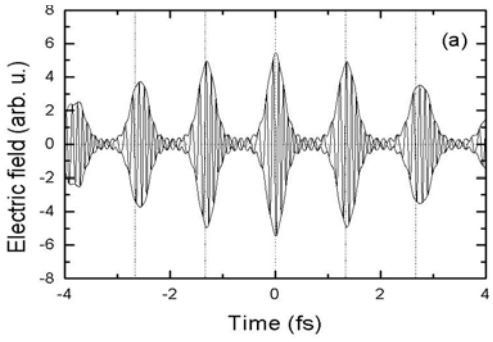

Már korábban ismert volt, hogy az attoszekundumos impulzus sorozat impulzusai a keltő lézerimpulzus véges volta miatt folyamatos változást mutatnak a femtoszekundumos időskálán. Ennek a változásnak a kvantitatív vizsgálatát végeztem el. Azt tapasztaltuk, hogy az impulzusok „követési távolsága" az impulzusok hossza illetve az impulzusok fázisa (CEP) a sorozat elemeiben különbözőek. A változást összefüggésbe hoztuk a harmonikus keltés során fellépő dipólfázis deriváltjaival, és megvizsgáltuk, hogy a változásért milyen mértékben felelős a lézerimpulzus adiabatikus, illetve nem-adiabatikus változása.

Szintén a nem-adiabatikus modell alapján vizsgáltuk szabad nemesgáz atomok által kibocsátott magasrendű harmonikusok spektrális és időbeli tulajdonságait. A femtoszekundumos és az attoszekundumos skálán is megfigyelhető fázismodulációt vizsgáltuk, ennek megfigyelhető következményeivel együtt. A chirp többféle megnyilvánulási módjai alapján számolt értékek jó egyezést mutatnak.

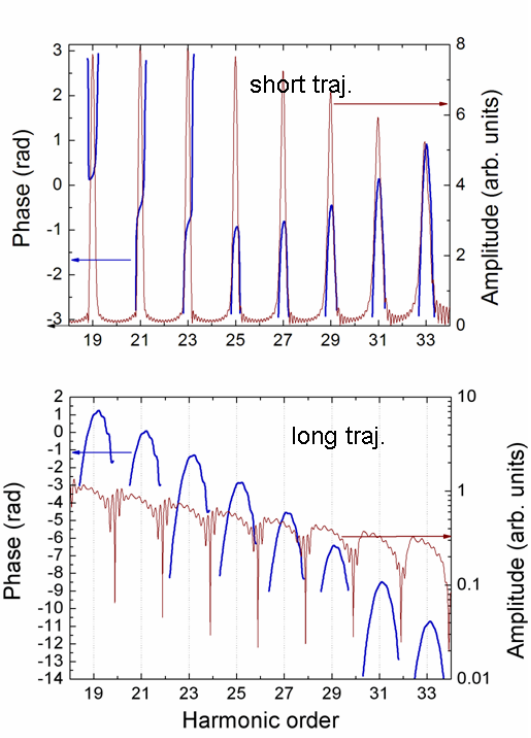

E témában elért eredményeinket két alkalommal mutattuk be nemzetközi konferencián:

K. Varjú, T. Ruchon, A. L'Huillier, P. Salières: *Saddle Point Approach For The Study Of HHG On Both Fs And As Timescales*, CG.2.2-MON at **CLEO/Europe-EQEC 2009**, Munich, June 14-19

K. Varjú, T. Ruchon, M. Mero, A. L'Huillier, and P. Saliéres: *Saddlepoint approach to describe high order harmonics in the temporal and spectral domain*, pp. 328-330 in Proc. **Ultrafast Optics VII, High Field Short Wavelength XIII**, Arcachon, Aug 31-Sep 4, 2009

A kutatás nyomán két kézirat is készült, melyet utolsó pontosítások után rövidesen referált folyóiratokhoz fogunk benyújtani (csatolva).

K. Varjú, T. Ruchon, Mark Mero, B. Carré, A. L'Huillier, and P. Saliéres: *Saddlepoint approach to describe high order harmonics generated in a noble gas on the femtosecond and attosecond timescales*

K. Varjú, T. Ruchon, Mark Mero, B. Carré, A. L'Huillier, and P. Saliéres: *Distortions of the attosecond pulse train generated by a multi-cycle laser beam*

2.3 Magasharmonikus keltés plazma felszínen

Nagy intenzitású lézertér szilárd felületen plazmát kelt, és a plazma nemlineáris oszcillációi magasrendű harmonikusok keltéséhez vezethet. Ez a módszer is alkalmas attoszekundumos impulzusok generálására. [Thaury *et al.*, Nat. Phys. **3**, 424 (2007)] A plazma harmonikusok előállításához nagyságrendekkel magasabb lézerintenzitásra van szükség, ezért ennek a folyamatnak a vizsgálata kezdetibb fázisban van, mint szabad gáz részecskék optikai ionizációja révén keltett harmonikus sugárzás megismerése. Ugyan a jelenség sokkal összetettebb, mint gázok esetén, mégis nagy jelentősége van ennek a módszernek, mert a lézer–

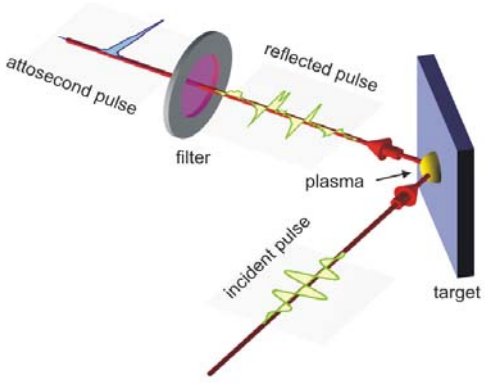

intenzitás növelésével ez a folyamat sokkal nagyobb intenzitású attoszekundumos impulzusok keltését teszi lehetővé.

A szilárd felszínen az intenzitástól függően többféle folyamat is lejátszódhat, melyek alapjában különböznek a gáz-fázisú részecskék optikai ionizációja révén keltett harmonikus keltés folyamatától, ezért ezeknek a folyamatoknak a vizsgálata most nagy érdeklődésre számot tartó terület.

Gáz harmonikusok esetében közismert, hogy a harmonikus keltés hatásfoka és a keltett harmonikusok polarizációja a lézerimpulzus polarizációs állapotától jelentősen függ, ami azért fontos, mert

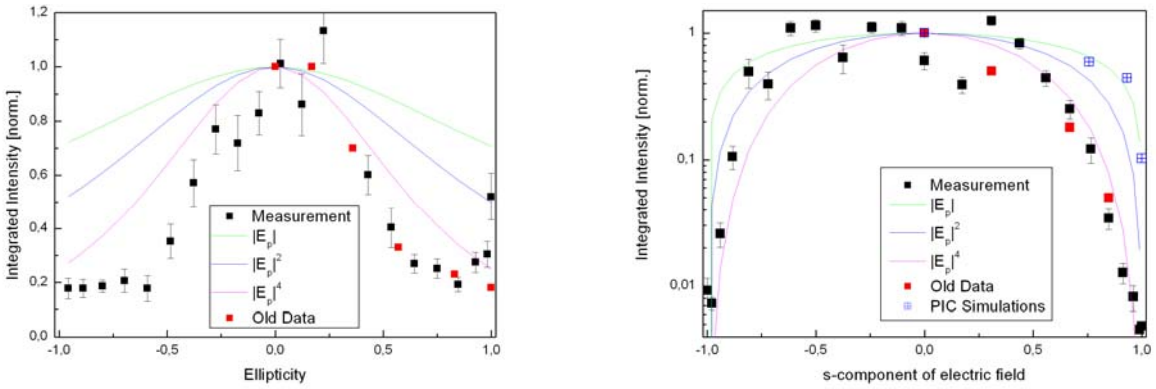

a lézerimpulzus ellipticitását időben változóvá téve elérhető, hogy a harmonikus-keltés ideje lényegesen rövidebb legyen, mint a lézerimpulzus hossza, ami izolált attoszekundumos impulzusok keltésére használható. Az MTA-RMKI (Budapest), MPQ (Garching, Germany), University 'Politehnica' of Bucharest kutatóival közösen azt vizsgáltuk, hogy a szilárd felszínen történő harmonikus keltés folyamatát hogyan befolyásolja a generáló lézerimpulzus polarizációs állapota. A kísérleteket Garchingban végeztük.

Első eredményeink azt mutatják, hogy mind az ellipticitás növelésével, mind a lineárisan poláris lézertér p-polarizációról s-re való átfordúláskor a harmonikusok intenzitása gyorsabban csökken, mint a szimuláció jóslata, vagyis a polarizációs időkapuzás plazma harmonikusok esetén is elképzelhető lehet.

A kísérletek kiértékelése még folyamatban van, az eredményeket további elemzések elvégzése után referált folyóiratban fogjuk közölni.

2.4 Attoszekundumos impulzusok keltése THz-es tér jelenlétében

Az attoszekundumos impulzusok létrejöttének feltétele, hogy a magas-harmonikus folyamat révén kellően széles spektrumú koherens sugárzást tudjunk kelteni. A spektrum kiterjesztése a keltő lézer impulzus intenzitásának vagy hullámhosszának növelésével érhető el. Az intenzitás növelése a keltő közeg kimerítésével jár, míg a hullámhossz növelésével a harmonikus keltés hatásfoka romlik.

Egy új javaslat szerint a spektrum kiterjeszthető úgy is, ha nagy erősségű, sztatikus elektromos tér jelenlétében keltjük a harmonikusokat [Y. Xiang, *et al.*, Physical Review A **79**, 053419 (2009)]. Ebben az esetben a harmonikus generálási folyamat már nem ismétlődik félperiódusonként, az egymást követő félperiódusok aszimmetrikussá válnak. Minden második félperiódusban az eredő elektromos térerősség

nagyobb, mint egyedül a lézertér esetében lenne, ezáltal a szabad elektronok nagyobb mozgási energiát nyerhetnek az elektromos tértől, és nagyobb frekvenciájú foton kibocsátása válik lehetővé. A másik félperiódusban természetszerűleg csökken a térerősség, és a spektrum is keskenyebbé válik, ezálzal a spektrumban két „cutoff" jelenik meg.

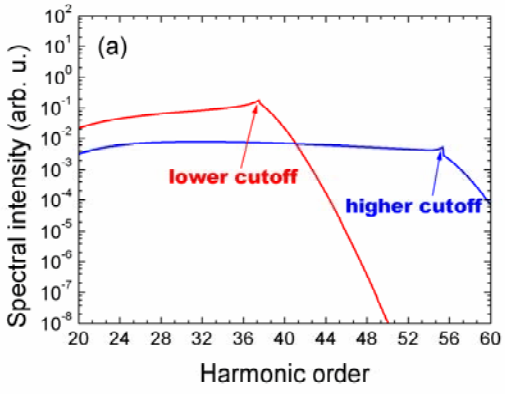

Ennek az elgondolásnak kísérletileg könnyebben megvalósítható módja, ha a lézerimpulzussal szinkronizált nagy intenzitású THz-es tér jelenlétében keltjük az attoszekundumos impulzusokat. Ezt a lehetőséget vizsgáltuk egy numerikus modell segítségével.

Az eredményeket egy absztraktban foglaltuk össze, melyet a CLEO konferenciára nyújtottunk be. (csatolva)

K. Varjú, J. A. Fülöp, P. Dombi, G. Farkas, J. Hebling:*Attosecond Pulse Generation in Noble Gases in the Presence of Extreme High Intensity THz Pulses*, **CLEO/QELS 2010: Laser Science to Photonic Applications**, May 16-21, 2010, San Jose McEnery Convention Center in San Jose, California

3 TÁRSADALMI HASZNOSÍTÁS – NYILVÁNOS FÓRUMON TÖRTÉNŐ BEMUTATÁS

Az ELI-nek köszönhetően jelentősen megnőtt kutatási területem iránti érdeklődés. Az elmúlt évben számos ismeretterjesztő szintű előadást tartottam:

1. Budó Ágoston Fizikai Feladatmegoldó Verseny középiskolásoknak, az eredményhirdetésen a legeredményesebben versenyző diákok és tanáraik számára előadást tartottam *Nemlineáris optikai jelenségek* címmel.
2. A Magyary Zoltán és OTKA Posztdoktori Öszöndíjasok tudományos eredményeit bemutató találkozón előadást tartottam *Attoszekundumos impulzusok* címmel
3. A III. Hungarian ELI Symposium (KFKI) meghívására előadást tartottam *Attosecond pulse generation* címmel
4. A MAGYAR TUDOMÁNY ÜNNEPE: Nagyintenzitású lézerfizikai kutatások Szegeden előadássorozat keretében előadást tartottam *Attoszekundumos impulzusok* címmel

4 KÖZLÉS ALATT ÁLLÓ PUBLIKÁCIÓK

A pályázat révén támogatott időszak mindössze 12 hónap volt. Ez az idő rövidnek bizonyult a kutatás elvégézése után az eredmények folyóiratban történő közlésére. Kérem, hogy a beszámoló értékelésénél vegyék figyelembe az elért eredmények későbbiekben történő publikálását is. Az elkészült kéziratokat az alábbiakban mellékelem.

Compression methods for XUV attosecond pulses

Katalin Varjú,[1,*] Mark Mero,[2] Fabio Frassetto,[3] Luca Poletto[3] and Paolo Villoresi[3]

[1] *Department of Optics and Quantum Electronics, University of Szeged, 6720 Szeged, Dóm tér 9., Hungary*

[2] *HAS Research Group on Laser Physics, University of Szeged, 6720 Szeged, Dóm tér 9., Hungary*

[3] *LUXOR Laboratory for UV and X-Ray Optical Research, CNR-INFM and Department of Information Engineering, University of Padova, Via Gradenigo 6/B, 35131 Padova, Italy*

[*] *Corresponding author: paolo.villoresi@unipd.it*

High order harmonic generation (HHG) is the prevailing method for the production of ultrashort pulses in the extreme-ultraviolet (XUV) and soft x-ray domains. The broadband coherent harmonic radiation supports optical pulses of attosecond duration. XUV pulses generated in gases via HHG carry an intrinsic positive chirp. Compression of attosecond pulses has been demonstrated using metallic transmission filters, a method with very limited tunability.

We discuss here the applicability of an XUV Attosecond Compressor (XAC): the two-grating configuration is a versatile method for temporal shaping of XUV radiation. We compare the compression achievable with XAC and metallic filters on simulated HH spectra.

OCIS codes: 050.1950, 190.4160, 260.7200, 320.0320, 320.5520, 320.5540.

1. Introduction

In the interaction of intense laser pulses and rare gases, high order harmonics are produced, transforming all the desirable properties of the generating laser pulse to the XUV and soft X-ray regime. Although the conversion efficiency is low, short duration, high degree of coherence and focusability make the produced harmonics an excellent source of short wavelength radiation. Also the broad bandwidth supports the production of attosecond pulses. The access to this unexplored time domain opens new frontiers in atomic, molecular and solid-state science, and new experiments with an unprecedented time resolution become possible.

XUV attosecond pulses, produced via high order harmonic generation in gases, possess a positive chirp, intrinsic to the generation process [1, 2], leading to longer than transform-limted pulses. To increase the usefulness of these pulses phase shaping has to be achieved. Thin metallic filters have constituted a simple and effective way to compensate the intrinsic chirp of XUV attosecond pulses [2, 3]. There is, however, a considerable disadvantage: metallic filters exhibit negative GDD only in well-defined wavelength regions (just above the absorption band), i.e. this method has a very limited tunability. Additionally, the transmission of the XUV radiation is strongly reduced by absorption.

The method presented here provides an alternative solution for the temporal compression of XUV attosecond pulses by controlling the GDD by means of a double-grating compressor. The design of the XUV Attosecond Compressor (XAC) [4], originates from the scheme of an XUV Time-delay Compensated Monochromator

([5]- [7]), realized to select a suitable portion of the HH spectrum within a broad spectral interval without altering the intrinsic pulse shape. We test here the applicability of the pulse shaper on simulated HH radiation, and also compare the pulse compression capability of the XAC to that of metallic filters. We note here, that in the XAC scheme both positive and negative GDD may be introduced, so not only pulse compression, but pulse shaping in general can be achieved.

2. Synthesis of an attosecond pulse

High order harmonic generation in rare gases is a result of an electronic process: after optical ionization, the electron is accelerated in the laser field, then recaptured by the parent ion, emitting its excess energy in form of an XUV photon. The properties of the radiation is inherited from the electron. The quantum mechanical description of the generation process makes use of certain simplifications, such as the one-electron and strong field approximations. The simulated XUV fields presented in this paper are calculated via a nonadiabatic version [8] of the saddlepoint method [9].

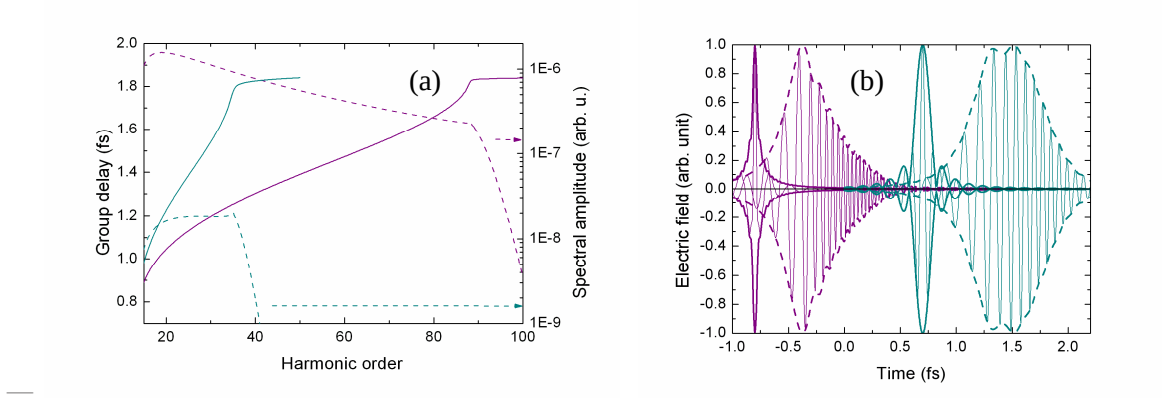

Fig. 1. (a) Spectrum and group delay of the high order harmonic radiation produced at a generating intensity of $1.5 \cdot 10^{14}$ W/cm^2 (green) and $6 \cdot 10^{14}$ W/cm^2 (purple). (b) Corresponding attosecond pulses possessing an intrinsic chirp (dashed lines) and their Fourier limit (solid lines).

Using long laser pulses for the generation process, a sequence of peaks corresponding to odd harmonics is produced in the spectrum, which corresponds to a series of attosecond pulses separated by half period in the time domain [10]. Harmonic generation with few cycle pulses, combined with ellipticity [11] or intensity gating [12] of the radiation allows to limit harmonic generation to a single half cycle, leading to the production of an isolated attosecond pulse, i.e. a selection of one pulse from the train.

In the simulation we consider a short, Gaussian sine type driving pulse of duration 25 fs, and numerically limit HHG to the first half cycle after the peak - only to produce continuous spectra and GD curves. The central wavelength of the pulse is 790 nm. We present attosecond pulses produced at generating peak intensities 1.5×10^{14} and 6×10^{14} W/cm^2 in neon gas.

The generated spectra together with the group delay (GD) values are shown in Figure 1. We have determined an average GDD for these two cases as $13 \cdot 10^{-3}$ fs^2 and $3.7 \cdot 10^{-3}$ fs^2. We observe that with increasing intensity the cutoff moves towards higher frequencies, and the value of the chirp decreases. We show in

Figure 1 the produced attosecond pulses, and their Fourier limit. As the spectral range increases and the chirp decreases, we get a shorter attosecond pulse for the higher generating intensity.

3. Compression by metallic filters

Close to absorption resonances material dispersion can be negative, which can be exploited to compensate the pozitive chirp of the generated attosecond pulses. Matching the generating intensity (and consequently the generated spectrum) to the material properties one can achieve compression of attosecond pulses close to the Fourier limit [2, 3].

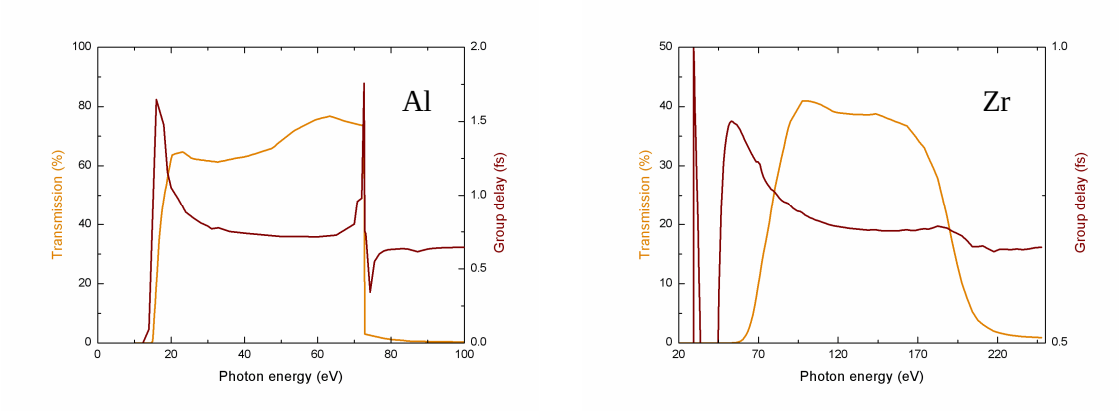

Fig. 2. Transmission and group delay of a 200 nm thick Aluminum / Zirconium filter.

Aluminum transmits radiation in the 20 - 70 eV region and at the onset of the transmission curve the filter possesses a negative GDD as shown in Figure 2. A laser pulse of intensity $1.5 \cdot 10^{14}\mathrm{W/cm^2}$ generates high harmonics in neon in this spectral range. Appropriately choosing this thickness of the filter, one can minimize the GDD, and therefore the pulse duration of the XUV pulses. In this case study we have found a minimal pulse duration when 1000 nm of aluminum filter was used.

Zirconium works as a bandpass filter in the 70 - 160 eV region, where we produce our high harmonics at a laser intensity $6 \cdot 10^{14}\mathrm{W/cm^2}$. We have found a minimal pulse duration with 1500 nm of Zr filter.

Pulseshapes after transmission through these filters are shown in Fig. 3 (orange curves).

Please note, that the use of filters shapes the spectrum as well as the group delay of the pulses, that affects pulse shaping. Furthermore, we use the filters close to their absorption, so with increasing thickness the throughput of the radiation decreases. We optimized the filter thickness for best compression, and found, that the peak intensity is reduced to 5% for aluminum and even further, about 10^{-5} times the unshaped case for zirconium. Using thinner filters allows higher transmission at the cost of less compression.

4. Compression by an XUV attosecond compressor

In the XAC gratings our mounted for grazing incidence, to increase reflection in the XUV domain, utilizing conical diffraction, where the incident and diffracted wave vectors are almost parallel to the grooves. The geometry is shown in Fig. 4a: the direction of the incoming rays is described by two parameters, the altitude γ and the azimuth α. All the rays leave the grating at the same altitude at which they approach. The azimuth α of the incoming rays is defined to be zero if they lie in the plane perpendicular to the grating surface and

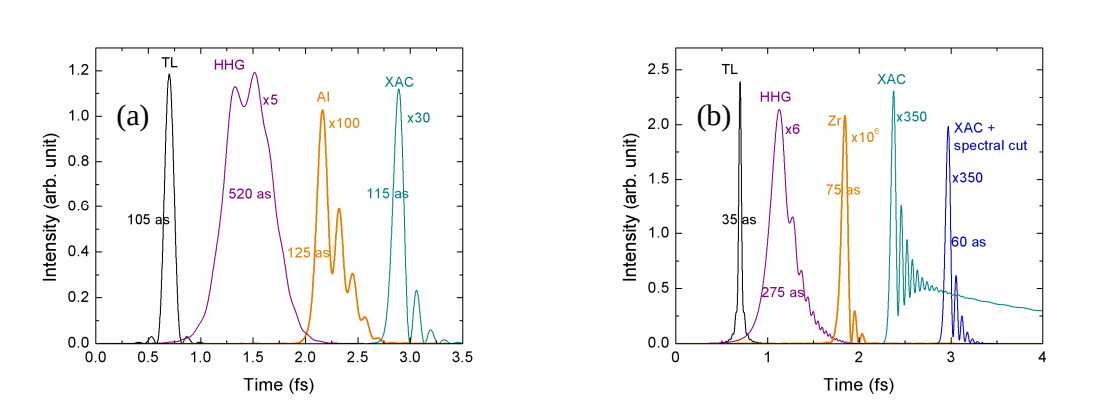

Fig. 3. Attosecond pulse generated at (a) $1.5 \cdot 10^{14}$ W/cm^2[(b) $6 \cdot 10^{14}$ W/cm^2]. Fourier limited duration is 105 as [$35as$], the pulses are generated with a duration of 520 as [$275as$], and we compress it in 1000 nm of Aluminum to 125 as [in 1500 nm of Zirconium to 75 as] with a considerable shoulder. Best compression with XAC provides pulses 115 as [$60as$] long. For better clarity the pulses are shifted in time.

parallel to the rulings, so $-\alpha$ is the azimuth of the zero-order light. β defines the azimuth of the diffracted light at wavelength λ and order m. The grating equation is written as:

$$\sin\gamma(\sin\alpha + \sin\beta(\omega)) = m\lambda\sigma, \tag{1}$$

where σ is the groove density.

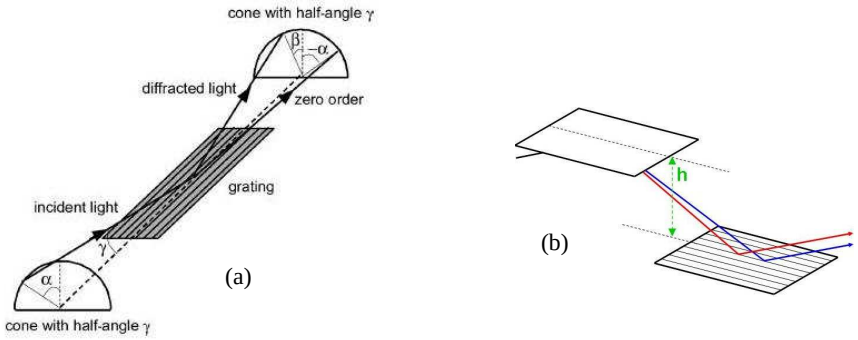

Fig. 4. (a) Grating in the off-plane mount. (b) XAC compressor built from two gratings at a normal distance h.

The XAC arrangement consists of two identical gratings, aligned at the same altitude. The azimuth angle α_1 of the incident rays on G1 is the same for all the wavelengths and gives the wavelength of maximum diffraction efficiency $\lambda_B = 2\sin\gamma\sin\delta/\sigma$ with $\beta_1(\lambda_B) = \alpha_1 = \delta$. The azimuth angle $\beta_1(\lambda)$ of the rays diffracted from G1 at different wavelengths is calculated from Eq. (1). The beam propagates toward the

second grating placed at a normal distance h (see Fig. 4b). Due to the symmetry of the configuration, the azimuth angle $\beta_2(\lambda)$ of the rays diffracted from G2 is constant with the wavelength and equal to α_1, so all the exit rays are parallel.

Adapting the method described in [13] we calculate analytically the GDD introduced by the two grating arrangement. The phase response is given by

$$\Psi(\omega) = \frac{\omega h}{c \sin\gamma \cos\beta(\omega)} \left\{1 + \cos\left[\pi - \cos^{-1}\left(\sin^2\gamma \cos(\alpha - \beta(\omega) + \pi) + \cos^2\gamma\right)\right]\right\} - 2\pi h\sigma \tan\beta(\omega), \qquad (2)$$

where we used the same notation as in [4], except for h, the perpendicular distance between the two gratings. Differentiation gives the GD, GDD and TOD.

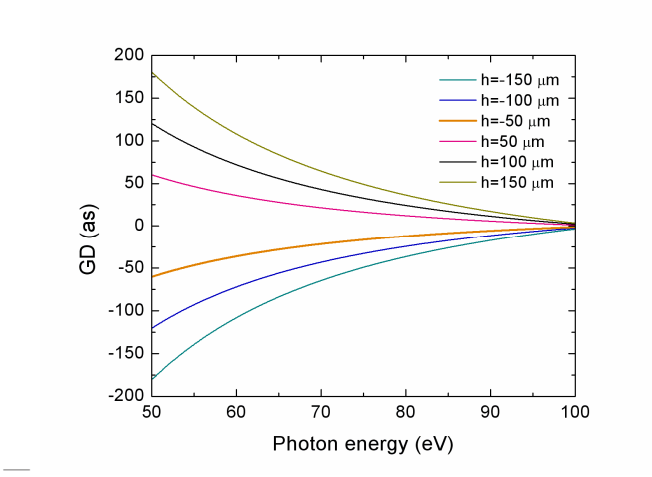

Fig. 5. GD obtained with the XAC at various grating distances h. Parameters: $\sigma = 200$ mm^{-1}, $\alpha = 4.5°$, $\gamma = 1.5°$.

The analytic formula reproduces the GD curves obtained with the ray tracing algorithm in [4], and proves that the GD is proportional to the grating distance, as speculated in the previous publication. We would like to note here, that this analytic formula applies for the chief ray, i.e. the ray emerging from the optical axis, and enables fitting certain parameters of the setup for optimal GD compensation. It cannot however account for off axis rays, so aberrations of the optical system must be accounted for by the ray tracing algorithm, as in [4].

In the actual XAC design [4] there are four additional parabolic mirrors in grazing-incidence, to collimate and refocus the XUV radiation such that the gratings are operated in parallel light. The XUV source is located at the front focal point, and all the rays are collected at the focus of the last mirror, while a spectrally dispersed image of the source is obtained in the intermediate plane. The two mirrors placed between the gratings act as a telescopic arrangement, thus we have $S' = S - (f_2 + f_3)$ where S is the chief ray optical path between the two gratings, and $h = S' \times \sin\gamma \cos\beta(\omega_0)$. This makes it possible to produce an effectively negative grating separation, continously tuning the GD(ω) from negative to positive values.

In contrast to double-pass compressors, here we have only a single pass: the different colours are focussed and overlap only at the focal point.

Using the ray tracing algorithm we optimize the grating parameters to minimize aberrations of the setup. We obtain that for the photon energy range 20-70 eV produced by the $1.5 \cdot 10^{14}$ W/cm^2 intensity laser pulse use of $\sigma = 200$ mm$^{-1}, \alpha = 4.5^\circ, \gamma = 1.5^\circ$ is desirable. Comparing the intrinsic GD curve shown in Fig. 1 with that obtainable with the XAC (Fig. 5) one can see that it is not possible to produce a transform limited output, but using the analytic formula for the GD we can easily optimize the grating distance to produce the shortest pulse duration. We achieve the best compression at a grating separation $\Delta h = 160 \mu m$, producing a compressed pulse shown in Fig. 3 (green curve). The asymmetric side structures are due to the higher order chirp still present after the XAC.

As a consequence of the off-plane mount, we achieve a photon throughput much higher than that of a conventional two grating configuration. The presented XAC arrangement provides a spectrally flat transmission of about 20% (?). Amplitude shaping achievable by masking in the intermediate plane might also improve the output pulse shape.

For the other generating intensity, and therefore other photon energy range, we find the optimum grating parameters as $\sigma = 300 mm^{-1} \alpha = 3.5^\circ \gamma = 1.2^\circ$ ([4]). The best compression for this situation is achieved at $\Delta h = 200 \mu m$, the corresponding pulse presented in Fig. 3 (green curve). We notice that the compressed pulse has a very strong asymmetric shoulder, because in this very broad bandwidth we cannot compansate the higher order dispersion. For better comparison with the metallic filter case we introduce a spectral cut between photon energies 75 eV and 190 eV similar to that imposed by the transmission of Zr (blue curve).

The transmission of the XAC setup has a higher transmission then the metallic filters. The XAC has approximatelly 20% spectrally flat throughput.

5. Conclusions

In this paper, we have tested methods for the compression of chirped, broadband attosecond pulses. Varying the grating separation in the XAC or the thickness of metallic filters allows one to tailor the GD of the XUV pulses, to a certain limit. These methods can be used to compress, or tailor the pulse shape, imposing a wide range of chirps

We find that when a material can be choosen to match in transmission and GDD the generated harmonic range the two methods achieve comparable compression. But the XAC is obviously more versatile in producing positive or negative chirps of variable magnitude and in the desired spectral range. And even more importantly it has throughput higher by orders of magnitude.

We have found that even with the XAC the intrinsic chirp of the attosecond pulses cannot be arbitrarily tuned. The corresponding residual GD and the spectrum is shown in Figure 6.

The existence of an intermediate plane in the XAC arrangement, where the radiation is spectally dispersed, however, enables further tailoring. We propose to insert a deformable mirror in the intermediate plane, which allows a small, but arbitrary phase shaping.

6. Acknowledgments

KV acknowledges the support of an OTKA/NKTH (H07B 74250) Postdoctoral Fellowship .

References

1. Y. Mairesse, *et al.*, *Attosecond Synchronization of High-Harmonic Soft X-rays*, Science 302, 1540.
2. R. López-Martens, *et al.*, *Amplitude and Phase Control of Attosecond Light Pulses*, Phys. Rev. Lett. , **94**, 033001 (2005).
3. E. Gustafsson, *et al.*, *Broadband attosecond pulse shaping*, Opt Lett **32**, 1353 (2007).

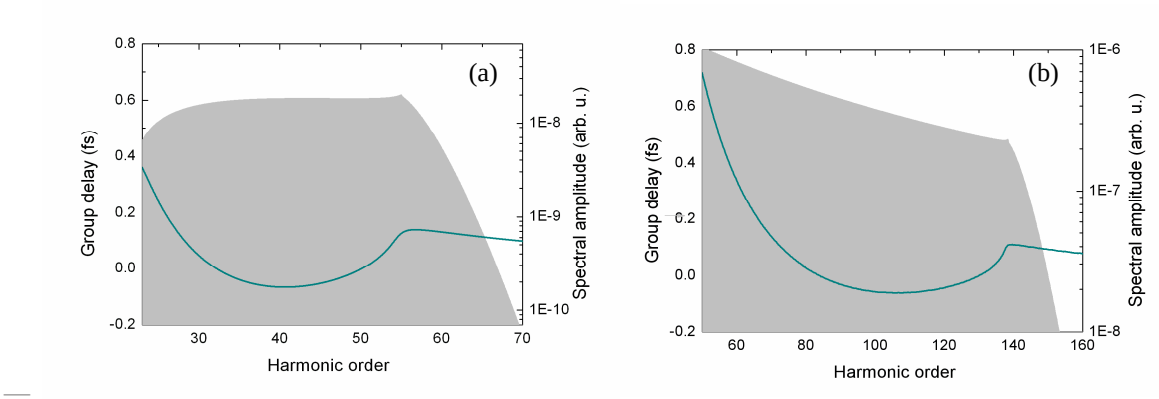

Fig. 6. Residual GD of the attosecond pulses generated at peak intensities (a) $1.5 \cdot 10^{14}$ W/cm^2[(b) $6 \cdot 10^{14}$ W/cm^2] after compression by XAC. Shaded grey areas indicate the high hamonic spectrum.

4. F. Frassetto, P. Villoresi, L. Poletto, *Optical concept of a compressor for XUV pulses in the attosecond domain*, Opt. Express , **16**, 6652 (2008).
5. P. Villoresi , *Compensation of optical path lengths in extreme-ultraviolet and soft-x-ray monochromators for ultrafast optics*, Appl. Opt., **38**, 28 (1999).
6. L. Poletto, P. Villoresi, *Time-delay compensated monochromator in the off-plane mount for extreme-ultraviolet ultrashort pulses*, Appl. Opt., **45**, 34 (2006).
7. L. Poletto, P. Villoresi, E. Benedetti, F. Ferrari, S. Stagira, G. Sansone, M. Nisoli, I*ntense femtosecond extreme ultraviolet pulses by using a time-delay-compensated monochromator*, Opt. Lett., **32**, 19 (2007).
8. G. Sansone, C. Vozzi, S. Stagira and M. Nisoli, Phys Rev A **70**, 013411 (2004).
9. M. Lewenstein, P. Salières, Phys Rev A **49**, 2117.
10. P. Villoresi , *Harmonic Generation in Gases*, Nonlin. Sources, OPTC00859 (2004).
11. I. Sola, *et al.*, *Controlling attosecond electron dynamics by phase-stabilized polarization gating*, Nature Phys **2**, 319 (2006).
12. R. Kienberger, *et al.*, *Atomic transient recorder*, Nature **427**, 817 (2004).
13. J-C. Diels and W. Rudolph, *Ultrashort laser pulse phenomena*, Chapter 2.6.2, Academic Press, San Diego (1996).

Saddlepoint approach to describe high order harmonics generated in a noble gas on the femtosecond and attosecond timescales

K. Varjú,[1] T. Ruchon,[2] Mark Mero,[3] B. Carré,[2] A. L'Huillier,[4] and P. Salières[2]

[1]*Department of Optics and Quantum Electronics, University of Szeged, 6720 Szeged, Dóm tér 9., Hungary*
[2]*CEA/DSM/DRECAM/SPAM, Bât. 522, Centre d'Etudes de Saclay, 91191 Gif-sur-Yvette, France*
[3]*HAS Research Group on Laser Physics, University of Szeged, 6720 Szeged, Dóm tér 9., Hungary*
[4]*Department of Physics, Lund Institute of Technology, P. O. Box 118, SE-221 00 Lund, Sweden*

This paper shall describe the possibilities opened by a saddlepoint discussion: like easy separation of short and long trajectory components, isolating the attosecond pulses in the train (characterisation-wise). This will also be the "'platform"' to test the validity of the PRL Taylor-expansion: we derive analytic formulae for ACEP, GD, GDD of pulses within the train, and compare the analytic - PRL - nonadiabatic saddlepoint results.

PACS numbers:

When a laser pulse is focused to a high intensity in a rare gas jet, high-order harmonics of the driving field are generated [1]. These harmonics serve as a broadband XUV radiation source enabling the production of attosecond pulses[2].

We understand the high order harmonic generation mechanism as a three-step process where an electron is teared off from the atom, accelerated in the laser field, and then recaptured while emitting the excess energy in form of a high-energy photon [3, 4]. Letting aside the macroscopic phase matching effects, many properties of the XUV radiation are inherited from the field-driven electron dynamics. The evolution of the free electron in the laser field can be approximated in a classical model [5], the main characteristics of the temporal structure of the attosecond pulses is obtainable: electrons of different kinetic energy return at different times, leading to a varying emission time (group delay) for the different energy components of the XUV pulse. The instant of ionization (i.e. the phase of the driving field) unambigously determines the kinetic energy of the returning electron, and the time of return. We might say, that these three parameters specifies the electron path, and they are strongly related/coupled.

SADDLEPOINT APPROACH

A fully quantum mechanical description of the harmonic generation process is presented in [6, 7], which has been further developed [9] to account for nonadiabatic effects arising when short driving pulses are used. The results presented in the present paper has been obtained using the method described in these references. The dipole moment of the electron producing the XUV radiation is given as

$$x(t) = i\int_{-\infty}^{t} dt' \int d^3p E(t') d_x^*(p - A(t)) \times d_x(p - A(t'))exp(-iS(p,t,t')) + c.c. \quad (1)$$

where p is the canonic momentum, t' is the ionistaion time and t is the time of recombination. $d_x(p)$ is the dipole matrix element, corresponding to ionisation (recombination) to a momentum state characterised by p. The phase term accumulated in the continuum state is the same as the classical action:

$$S(p,t,t') = \int_{t'}^{t} dt'' \left(\frac{(p - A(t''))^2}{2} + I_p \right) \quad (2)$$

Here $A(t)$ is the vector potential corresponding to the fast varying electric field given as:

$$E(t) = E_0 \cdot \left(cos\left(\frac{t}{\tau}\right)\right)^2 \cdot cos(\omega t + \psi) \quad (3)$$

where ω is the carrier component of the fundamental frequency, ψ is the carrier envelope phase, and $cos\frac{T}{2\tau} = (2^{-1/4})$ where T is the FWHM duration of the driving pulse.

The harmonic pulses presented here are generated in Neon, by a 30 fs pulse, with a peak intensity $2 \cdot 10^{14}$ W/cm^2.

In Eq. (1) we identify the ionisation and recapture process and the evolution of the electron wavepacket in the laser field in the integrand. The stationary action principle applied to the harmonic dipole phase results in three coupled saddlepoint equations:

$$\begin{aligned} p_s &= \tfrac{1}{t-t'} \textstyle\int_{t'}^{t} A(t'')dt'' \\ q\omega - \tfrac{(p_s - A(t_s))^2}{2} - I_p &= 0 \\ \tfrac{(p_s - A(t'_s))^2}{2} + I_p &= 0 \end{aligned} \quad (4)$$

describing momentum and energy conservation for the generation process [6, 9]. The solutions to these will describe all possible electron trajectories. Each trajectory is characterized by the three parameters, namely ionization time (t'), return time (t) and momentum (p), and these values unambiguously define the electron trajectories, and hence the corresponding dipole. In each half cycle we get two classes of solutions for each q value, used as a continuous parameter. For each of these trajectories we can determine the dipole moment, ξ_q^j indexed by q (harmonic order) and j trajectory class:

$$\xi_q^j = \frac{i2\pi}{\sqrt{det(S'')}}\left[\frac{\pi}{\epsilon+i(t_s-t_s')/2}\right]^{3/2} \times E(t_s')d_x^*(p_s - A(t_s))d_x(p_s - A(t_s')) \times exp(-iS(p_s, t_s, t_s') + i\omega t_s) \quad (5)$$

In Figure 1 we plot the XUV photon energy as a function of return time. The usual conclusions can be drawn from such a plot: in each optical cycle there are two trajectories leading to the same energy photon, the so-called short and long trajectories. The two trajectories merge at the cutoff, the position of what varies along the pulse, together with the driving laser pulse envelope. The slope of the curve made up from short trajectory components has an opposite sign, as compared with the long trajectory class, corresponding to opposite chirp in the two cases.

We would like to emphasize here, that in this Figure, each point of the curves represents an electron trajectory, and this illustration helps to categorize them. All short trajectory components are plotted in blue, and long trajectories in orange. Trajectories contributing to the emission of a certain spectral range can be identified as points within a horizontal structure, and emission in a temporal slot can be obtained from trajectories in a vertical section.

The spectrum of harmonic radiation is then given as the Fourier transform of $x(t)$, which is reduced to a sum of the contribution from the "relevant" quantum trajectories.

$$x_q = \sum_s \xi_q^j \quad (6)$$

The key word here is: relevant. A great advantage of this approach is, that the relevance of the trajectories is defined for each physical situations. For a given driving pulse we solve the saddlepoint equations for each half cycle, to obtain a set of solutions. Summing all the solutions provides the total harmonic radiation, but to gain a specific information about the radiation, we can restrict summation over a class of solutions (trajectories).

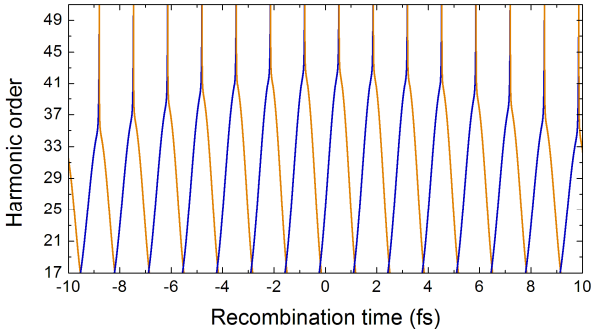

FIG. 1: Harmonic photon energy as a function of the recombination time, solutions of the saddlepoint equations.

SHORT AND LONG TRAJECTORIES

In the interaction of a single atom with the laser pulse, both short and long trajectory components are generated, and this is what we describe in the model presented here. When harmonics are generated experimentally, it is the macroscopic sum of the radiation produced by the individual atoms or molecules. Since the phase behaviour of the short and long trajectories are very different, phase matching in the extended medium always favours one trajectory class, so the produced radiation is dominated by radiation from one trajectory class. [8, 16]

In the saddlepoint approach, it is very easy to separate the short and long trajectory components (based on e.g. the value of the return time), and hence compare the properties of the radiation produced via either trajectory class, as shall be done in the following sections.

FEMTOSECOND CHARACTERISATION OF THE HARMONIC RADIATION

As explained in our previous paper [10], the femtosecond characteristics of the harmonic radiation arises from the variation of the intensity of the generating laser pulse, and is observable on the individual harmonics. To investigate the extent of this effect, for each harmonic order we sum up all trajectories contributing, i.e. the summation in Eq. 6 is along horizontal sections of Figure 1, i.e. on the index j. In fact, for the femtosecond characterisation we don't have a continuous time parameter, but rather, we are sampling each harmonic at the discrete return time instants, so we have

$$x_q(t) = \xi_q^j \texttt{ at } t = t_q^j \quad (7)$$

As the magnitude and phase of x_q varies from cycle to cycle along the driving pulse, i.e. on the femtosecond timescale, enables us to describe the harmonic emission on the femtosecond scale.

It has been seen both experimentally, and theoretically[10, 11], that the generated harmonics are chirped, i.e. there is a streaking of frequency with time, arising from the change of the driving intensity. Using the saddlepoint solutions, it is possible to determine the harmonic spectrum generated at different parts of the fundamental pulse by summing only in a selected range of cycles. Figure 2 shows the spectra resulting from short and long trajectory components at four different segments/temporal window of the driving pulse. The parts of the laser pulse is colored red at the beginning, then green, orange and blue at the falling end. The top figure shows the spectra produced by short trajectories. For the 21st harmonic there seems to be no shift of the peak, corresponding to zero chirp. The harmonic below shows a very small positive chirp, while the harmonics above show a negative chirp that increases with harmonic order. The middle figure shows the spectra for the long trajectories. Here the chirp is negative for all harmonics, and higher in magnitude than in the case of the short trajectory. As shown in [10], the chirp of the harmonics can be expressed as

$$b_j^q = 8\ln(2)\,\frac{\partial\Phi_j^q}{\partial I}\,\frac{I_0}{\tau_0^2}. \tag{8}$$

q	19	21	33	35
b short (10^{28}fs^{-2})	0.8549	0.223	-6.266	-8.017
b long (10^{28}fs^{-2})	-41.21	-40.72	-35.08	-33.47
$\frac{\Delta\omega}{\Delta t}$ short (10^{28}fs^{-2})	0.688	0.137	-6.6	-8.8
$\frac{\Delta\omega}{\Delta t}$ long (10^{28}fs^{-2})	-34.8	-34.4	-28.1	-25.7

TABLE I: Comparison of the chirp values deduced from equation 8 and the peak shift in Figure 2.

ATTOSECOND CHARACTERISATION OF THE HARMONIC RADIATION

Focusing to the short term characteristics of high order harmonic radiation, one finds that the radiation is bunched into attosecond pulses. It has been proven experimentally, that these attosecond pulses are chirped, i.e. the frequency is streaked in time, the harmonic components are delayed relative to each other. The same characteristics is seen in Fig. 1, looking at the electron trajectories that result in emission within an optical cycle. There are two branches of trajectories, in both of them return time varies with photon energy, meaning that the components are emitted with a varying delay. For the short trajectory class frequency increases with time, resulting in positively chirped pulses, whereas for the long trajectory class we expect negatively chirped pulses. Also, the return times for the two classes are

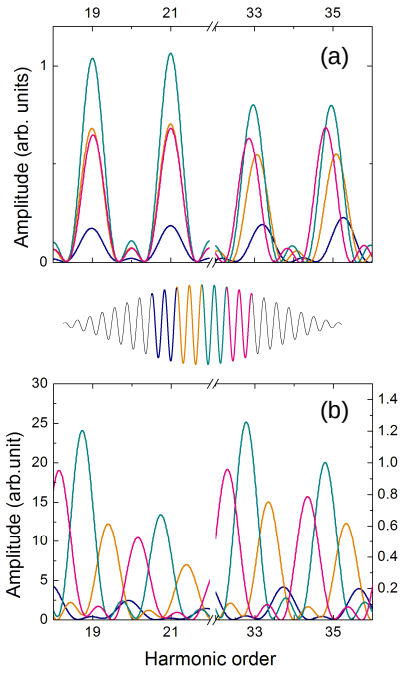

FIG. 2: Harmonic spectra generated at different portions of the 25 fs laser pulse of peak intensity 2×10^{14} W/cm^2 in Neon.

different, so we expect to observe the short and long trajectory pulses shifted in time.

To study the attosecond pulses by means of this saddlepoint method, we sum up separately all short trajectory, and all long trajectory components. Applying Fourier transform for the spectrum given by Eq. 6, we obtain the two corresponding pulse trains, that we illustrate in Fig. 3. We observe that the pulses are delayed, and the timing of the pulses correspond to the return time of the carrier harmonic component. It is also clear from the illustration, that the two pulse trains consist of oppositely chirped pulses: for the short trajectory the instantaneous frequency of the bursts increases, for the long trajectory it decreases with time.

Using this method we can also compare pulses in different regions of the pulse train by summing electron trajectories in certain return time regions. It has been seen in [13] that there are pulses-to-pulse changes in the train in timing, chirp and ACEP. We show in Figure 4 two sections of the attosecond pulse train, generated via the short trajectory class.

SPECTRAL FEATURES

Summing all saddlepoint solutions in Eq. 1 provides the total harmonic spectrum. Restricting the sum to short or long trajectories allows to compare the two types of radiation spectrally. Already in Figure 2 we have seen that for the long trajectory there is a greater chirp and

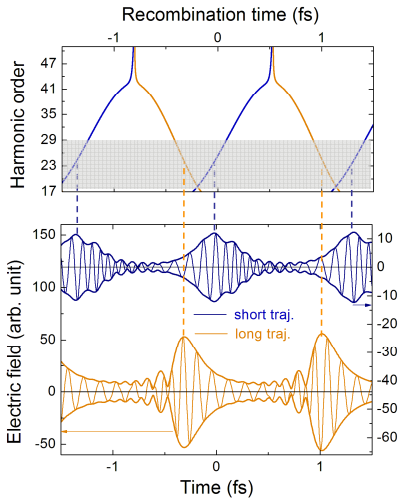

FIG. 3: Attosecond pulses generated through short and long trajectory components.

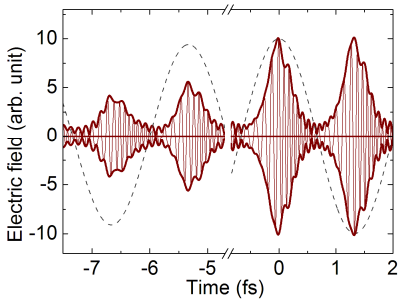

FIG. 4: Attosecond pulse train sections.

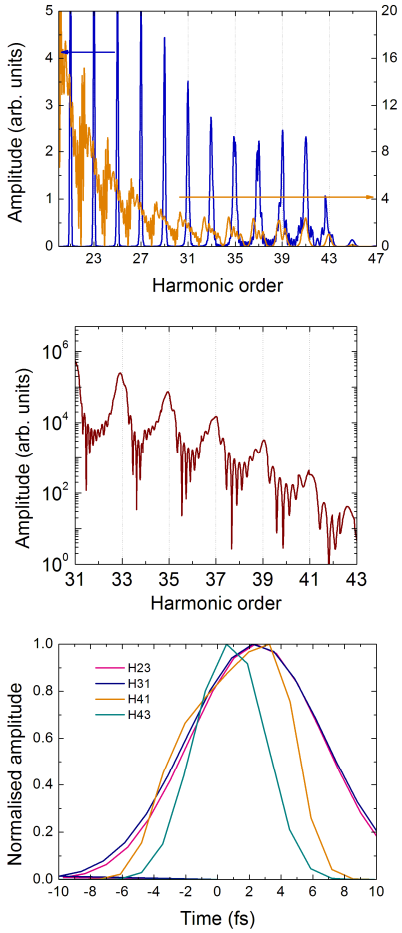

FIG. 5: (a) Harmonic spectra produced by short and long trajectory components. (b) Cutoff portion of the generated spectra in a logarithmic scale. (c) Individual normalised temporal shape of some of the generated harmonics.

thus the harmonic lines are supposed to cover a broader range. In Figure 5 we plot the two spectra: the long trajectory harmonics are so broad, that the adjacent lines overlap, and we observe the fringe pattern at the even orders described in [14].

It was shown in Figure 1 that for such short driving pulses the intensity and thus the cutoff position varies so rapidly pulse-to-pulse, that there is a considerable decrease in the number of half-cycles contributing to the emission of a harmonic with increasing harmonic order. This results in different temporal durations of the harmonic, which we see in the spectrum as narrow lines for the low orders and broader lines for the higher orders.

In Figure 5 (c) we indicate how the duration of the harmonic pulses change with harmonic order. For plateau harmonics we expect and we observe approximatelly the same pulse durations. As we are reaching the cutoff, the contributing half-cycles, and thus the duration of the harmonics decreases.

In a magnified section of the highest orders (Fig. 5 (b)) we also see side-maxima between the harmonic lines. The number of sidemaxima is decreasing with increasing harmonic order, corresponding to a reducing number of contributing half-cycles. [15]

In Figure 6 we plot the phase of the harmonic field (short trajectories). It clearly illustrates, that there is a chirp within the harmonic bandwidth, this is the harmonic chirp that was investigated in Fig. 2, that is negative in most cases, apart from the lowest orders: H19 appears to posses a positive chirp, and the phase of H21 varies linearly with order, i.e. it has no chirp. The higher orders all have a negative chirp, the magnitude increases with order. The phase values at the center of the harmonic lines also lie on an upward-pointing second order curve, corresponding to a positive atto chirp, which shows up in Figure 3. (This figure corresponds to Fig. 7 of [10], but it is not an artist's view anymore)

The phase of the dipole moment of Eq. 6 can be written as:

$$\Psi_q^j = \eta_q^j - S(p,t,t') + \omega t_q^j, \tag{9}$$

where η_q^j is the phase of the complex factors.

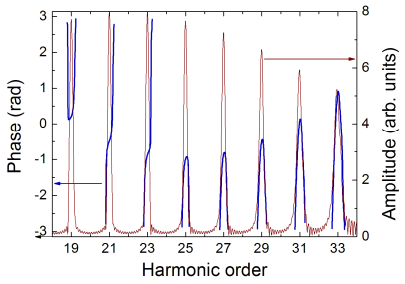

FIG. 6: Phase of the harmonic emission.

CONCLUSIONS

This research was supported by the Marie Curie European Program (MRTN-CT-2003-505138). KV acknowledges the support of the NKTH-OTKA and János Bolyai Postdoctoral Fellowships.

[1] M. Ferray *et al.*, J. Phys. B **21**, L31 (1988).
[2] G. Farkas, C. Tóth, Phys. Lett. A **168**, 447 (1992).
[3] K. Schafer, *et al.*, Phys. Rev. Lett. **70**, 1599 (1993).
[4] Corkum, Phys. Rev. Lett. **71**, 1994 (1993).
[5] Varju et al, American Journal of Physics
[6] Lewenstein, PRA 49, 2117.
[7] M. Lewenstein *et al.*, Phys. Rev. A **52**, 4747 (1995).
[8] Antoine, PRL 77, 1234.
[9] Sansone, PRA 70, 013411.
[10] K. Varjú *et al.*, J. Mod. Opt. **52**, 379 (2005).
[11] J. Mauritsson *et al.*, Phys. Rev. A **70**, 021801(R) (2004).
[12] P. Antoine, Phys. Rev. A **53**, 1725.
[13] K. Varjú *et al.*, Phys. Rev. Lett. **95**, 243901 (2005).
[14] Sansone, Phys. Rev. Lett. **92**, 113904 (2004).
[15] Mansten PRL.
[16] M. Bellini *et al.*, Phys. Rev. Lett. **81**, 297 (1998).

Distortions of the attosecond pulse train generated by a multi-cycle laser beam

K. Varjú,[1] T. Ruchon,[2] Mark Mero,[3] B. Carré,[2] A. L'Huillier,[4] and P. Salières[2]

[1]*Department of Optics and Quantum Electronics, University of Szeged, 6720 Szeged, Dóm tér 9., Hungary*
[2]*CEA/DSM/DRECAM/SPAM, Bât. 522, Centre d'Etudes de Saclay, 91191 Gif-sur-Yvette, France*
[3]*HAS Research Group on Laser Physics, University of Szeged, 6720 Szeged, Dóm tér 9., Hungary*
[4]*Department of Physics, Lund Institute of Technology, P. O. Box 118, SE-221 00 Lund, Sweden*

Pulses of the attosecond pulse train are characterized. We study pulse-to-pulse variation of ACEP, GD and GDD and connect the variation to the dipole phase derivatives. We test the adiabatic and non-adiabatic nature of the pulse distortions.

PACS numbers:

In the interaction of rare gases and intense laser pulses, an XUV spectrum of high harmonics is produced[1], broad enough to support the production of attosecond pulses. In case of few cycle generating laser pulses, and selection techniques based on intensity or ellipticity gating single attosecond pulses are produced. In the more general case a train of attosecond pulses is created[2, 3].

For a finite laser pulse the electric field of the laser pulse changes from cycle to cycle, leading to the producion of uneven bursts: the delay, chirp and carrier-envelope phase (ACEP) of the attosecond pulses vary from pulse to pulse [4, 5].

Measurement...[6, 7]

In our previous publication[4] we have presented an adiabatic phase expansion to characterize attosecond pulse trains in the multicycle time scale, and pointed out the variation of the pulse characteristics along the train. Here we advance on the question, presenting analytic formulae for the ACEP, GD and GDD variation of the pulses, discussing the physical parameters responsible for the distortions, and comparing the results with those obtained in a non-adiabatic model[11].

ADIABATIC DESCRIPTION

In the adiabatic model[4] we assume the generating pulse to be synthetised from constant-amplitude sine sections. The attosecond pulse train is produced by the coherent sum of the harmonics:

$$E_{XUV}(t) = \sum_{q=q_i}^{q=q_f} A_q(t) e^{-iq\omega t - i\Psi_q(t)}. \qquad (1)$$

where ω is the laser frequency, $A_q(t)$ and $\Psi_q(t)$ are the amplitude and phase of the qth harmonic, depending on time t. $|E_{XUV}(t)|^2$ consists of a train of pulses of duration a few hundred attoseconds, separated by half the laser period, spanning over an interval of few tens of femtoseconds. Eq. (1) treats differently the attosecond and femtosecond time scales of the problem: the femtosecond structure is expressed in the time domain, through the (slow) time variation of $A_q(t)$ and $\Psi_q(t)$. The attosecond electric field, on the other hand, is here characterized by the spectral variation of A_q and Ψ_q. The phase of the single-atom response

$$\Psi_q(t) + q\omega t = q\Phi_0(t) - \Phi_q(t) \qquad (2)$$

includes a contribution from the fundamental field $q\Phi_0(t)$, with

$$\Phi_0(t) = \omega t + \phi_0 + b_0 t^2/2 + \dots \qquad (3)$$

where ϕ_0 is the fundamental CEP and b_0 a possible frequency chirp, as well as phase terms originating from the generation process

$$\Phi_q(t) = \int_{t'}^{t} dt'' \frac{(p - A(t''))^2 + I_p}{2} - iq\omega t. \qquad (4)$$

Our reconstruction of the attosecond train uses a Taylor expansion up to fourth order of the phase term both in frequency Ω, covering the whole frequency range by discrete steps of 2ω and in time in the long femtosecond time scale. The Taylor expansion is performed around $(\Omega, t) = (q_0\omega, 0)$, where q_0 is the central harmonic order and $t = 0$ is the maximum of the laser pulse. The phase term originating from the generation process $\Phi_q(t)$ depends on time via the fundamental laser intensity envelope $I(t)$. Assuming that $I(t)$ is symmetric with respect to $t = 0$, all its odd derivatives around $t = 0$ are equal to zero. The third and fourth order terms in $(\Omega - q_0\omega)$, as well as the fourth order terms in t are found to be very small and can be neglected. We use the notation $\gamma = d^2I/dt^2$, at $t = 0$. For a Gaussian pulse characterized by a peak intensity I_0 and a pulse duration τ, $\gamma = -8\ln(2)I_0/\tau^2$. Writing the frequency derivatives as $\partial\Phi/\partial\Omega = 1/\omega\ \partial\Phi/\partial q$ we obtain:

$$\Phi_q(t) \approx \Phi_{q_0}(I_0) + \frac{\gamma t^2}{2}\frac{\partial\Phi}{\partial I} + (q - q_0)\frac{\partial\Phi}{\partial q} + \qquad (5)$$
$$\frac{(q-q_0)^2}{2}\frac{\partial^2\Phi}{\partial q^2} + (q - q_0)\frac{\gamma t^2}{2}\frac{\partial^2\Phi}{\partial q\partial I} + (q - q_0)^2\frac{\gamma t^2}{4}\frac{\partial^3\Phi}{\partial q^2\partial I}$$

In this equation, all the partial derivatives are taken at $q = q_0$ and $I = I_0$. The phase of the fundamental and the

effect of a phase modulation induced by the propagation through a medium with a constant group delay dispersion denoted by δ can be easily introduced. (We here neglect the group delay of the material, for the sake of simplicity, since it will just lead to an overall time shift).

$$\Phi_q^p(t) = \frac{\delta\omega^2}{2}(q-q_0)^2 \tag{6}$$

The total phase becomes

$$\begin{aligned}\Psi_q(t) + q\omega t \approx q_0\omega t - \Phi_{q_0}(I_0) + q_0\phi_0 + \left(-\tfrac{\gamma}{2}\tfrac{\partial\Phi}{\partial I} + q_0\tfrac{b_0}{2}\right)t^2 \\ + \left(-\tfrac{\partial\Phi}{\partial q} + \omega t + \phi_0\right)(q-q_0) - \left(\tfrac{1}{2}\tfrac{\partial^2\Phi}{\partial q^2} + \tfrac{\delta\ \omega^2}{2}\right)(q-q_0)^2 \\ + \left(-\tfrac{\gamma}{2}\tfrac{\partial^2\Phi}{\partial q\partial I} + \tfrac{b_0}{2}\right)(q-q_0)t^2 - \left(\tfrac{\gamma}{4}\tfrac{\partial^3\Phi}{\partial q^2\partial I}\right)(q-q_0)^2\ t^2\end{aligned} \tag{7}$$

Differentiation with respect to frequency gives a group delay of

$$GD = -\frac{1}{\omega}\left(\phi_0 - \frac{\partial\Phi}{\partial q} + \left(\frac{b_0}{2} - \frac{\gamma}{2}\frac{\partial^2\Phi}{\partial q\partial I}\right)t^2\right). \tag{8}$$

The second derivative corresponds to the group delay dispersion, or second order spectral phase:

$$GDD = \frac{2}{\omega^2}\left(\frac{1}{2}\frac{\partial^2\Phi}{\partial q^2} + \frac{\delta\ \omega^2}{2} + \frac{\gamma}{4}\frac{\partial^3\Phi}{\partial q^2\partial I}t^2\right). \tag{9}$$

This analytic formula for the phase enables us to derive an expression for the $ACEP$ values (by taking the phase of the carrier component Ψ_{q_0} at the peaks of pulses, i.e. $-q_0\omega\cdot GD$):

$$ACEP = -\Phi_{q_0}(I_0) + q_0\frac{\partial\Phi}{\partial q} - \left(\frac{\gamma}{2}\frac{\partial\Phi}{\partial I} - q_0\frac{\gamma}{2}\frac{\partial^2\Phi}{\partial q\partial I} + \frac{b_0}{2}\right)t^2. \tag{10}$$

These expressions allows a quick and easy characterisation of the APT with the knowledge of the phase derivatives[8]. These phase derivatives are calculated using the saddlepoint method introduced by Lewenstein[9, 10] for a monochromatic fundamental field. Tables I and II present some illustrative values for harmonic generation in argon and neon at two generating intensities and two harmonic orders for the short trajectories.

I (10^{14}W/cm^2)	1.5	2	1.5	2
q	23	23	27	27
Φ_{q_0}	34.712	34.548	47.793	46.999
$\partial\Phi/\partial I$ (10^{-14}W^{-1}cm^2)	-0.479	-0.221	-2.081	-1.223
$\partial\Phi/\partial q$	1.001π	0.957π	1.087π	1.03π
$\partial^2\Phi/\partial q^2$	0.07	0.059	0.067	0.053
$\partial^2\Phi/\partial q\partial I$ (10^{-14}W^{-1}cm^2)	-0.338	-0.218	-0.472	-0.285
$\partial^3\Phi/\partial q^2\partial I$ (10^{-14}W^{-1}cm^2)	-0.026	-0.012	-0.043	-0.017

TABLE I: Values of the spectral phase and phase derivatives at the **23rd** and **27th** harmonic of 800 nm radiation in **neon**.

I (10^{14}W/cm^2)	1.5	2	1.5	2
q	23	23	27	27
Φ_{q_0}	45.212	44.207	59.541	57.638
$\partial\Phi/\partial I$ (10^{-14}W^{-1}cm^2)	-2.588	-1.58	-5.031	-2.934
$\partial\Phi/\partial q$	1.098π	1.037π	1.192π	1.106π
$\partial^2\Phi/\partial q^2$	0.07	0.055	0.081	0.054
$\partial^2\Phi/\partial q\partial I$ (10^{-14}W^{-1}cm^2)	-0.497	-0.296	-0.76	-0.387
$\partial^3\Phi/\partial q^2\partial I$ (10^{-14}W^{-1}cm^2)	-0.048	-0.018	-0.12	-0.029

TABLE II: Values of the spectral phase and phase derivatives at the **23rd** and **27th** harmonic of 800 nm radiation in **argon**.

NON-ADIABATIC DESCRIPTION

For the non-adiabatic characterization we follow the method of Sansone[11]. A generating laser pulse of form

$$E(t) = E_0\cdot\left(cos\left(\frac{t}{\tau}\right)\right)^2\cdot cos(\omega t+\psi) \tag{11}$$

is chosen where ϕ_0 is the CEP, and $cos\frac{T}{2\tau} = (2^{-1/4})$ where T= 25 fs is the FWHM duration of the driving pulse. We simulate harmonic generation in neon, at a peak intensity of $2\cdot10^{14}$W/cm^2. Using the saddlepoint approximation we determine the trajectories with extrema of the action, carrying relevant contribution to the produced radiation. The attosecond pulse train is synthetized from the coherent sum of the dipole radiation corresponding to each short trajectory. The spectrum is shaped with a Gaussian filter of central harmonic $q_0 = 25$ and $\Delta q = 8$. The generated pulse train is illustrated in Fig. 1 at two CEP values. The pulse characteristics ACEP, GD and GDD are numerically determined from the phase of the simulated field.

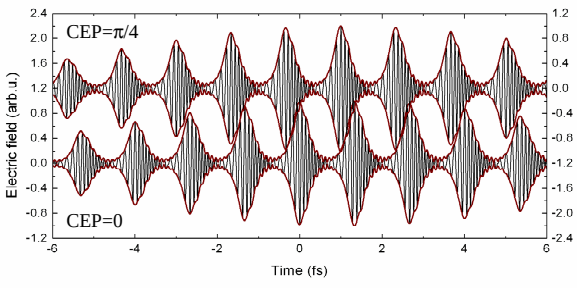

FIG. 1: Electric field of the pulse train generated at a peak intensity of 2×10^{14}W/cm^2 calculated using the non-adiabatic method for two values of the CEP.

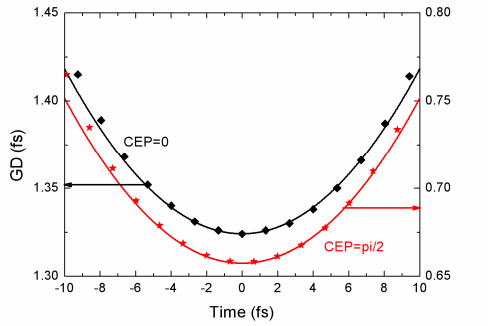

FIG. 2: GD values of the attosecond pulse train calculated from the adiabatic model (continouos line), and the non-adiabtic model (symbols) for two different CEP value.

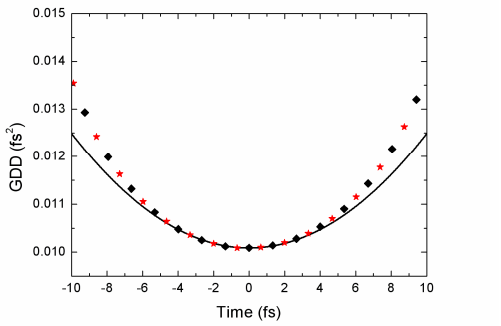

FIG. 3: GDD values of the attosecond pulse train calculated from the adiabatic model (continouos line), and the non-adiabatic model (symbols) for a 25-fs, $2 \cdot 10^{14}$W/cm^2-peak intensity laser pulse interactin with neon atoms.

COMPARISON OF THE ADIABATIC AND NON-ADIABTIC PULSE CHARACTERISTICS

Figures 2 -4 show the GD, GDD and ACEP variation of the attosecond pulses along the pulse train, calculated analytically for the adiabatic case (Eqs. 8-10), and numerically for the non-adiabtic case, for a 25 fs, $2 \cdot 10^{14}$W/cm^2 peak intensity, $b_0 = 0$ driving pulse, interacting with neon atoms.

In Fig. 2 we observe a very good agreement between the two models. Apart from a small deviation at the wings, the non-adiabatic values appear to follow the same behaviour, sampled at the pulse appearances. The curve shifts vertically with the change of CEP, corresponding to an overall delay of the pulse train cf. Fig. 1. The pulse-to-pulse variation is determined by the coefficient of the t^2 term in Eq. 2. The magnitude of the variation depends on the generating pulse parameters through b_0 and γ, and the peak intensity, generating gas and central harmonic through the phase derivative $\frac{\partial^2 \Phi}{\partial q \partial I}$. Using the data given in the tables, it is easy to determine that the amgnitude of the group delay variation increases with the central harmonic, and decreases with the pulse duration, and the increase of the ionization potential of the gas.

In case of $b_0 = \gamma \frac{\partial^2 \Phi}{\partial q \partial I}$ there is no change of the delay with time, i.e. an evenly spaced attosecond pulse train is generated[5, 8].

The GDD (related to the frequency chirp) of the attosecond pulses also show a parabolic behaviour. The discrete non-adiabatic values follow the same curve, independent of the CEP of the laser, but the points are shifted along the curve corresponding to the time shift of the trains. The temporal variation depends also on the generating pulse parameters and the choice of gas via the phase derivative $\frac{\gamma}{4} \frac{\partial^3 \Phi}{\partial q^2 \partial I}$. Using propagation through a filter, the GDD of all pulses can be shifted by the same amount. It is possible to achieve no chirp for the central pulse, but the pulses will possess an increasing amount

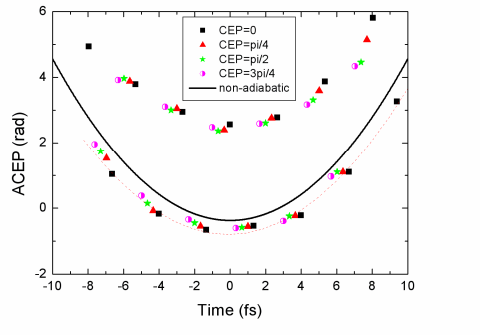

FIG. 4: ACEP values of the attosecond pulse train calculated from the adiabatic model (continouos line), and the non-adiabtic model (symbols) for a 25-fs, $2 \cdot 10^{14}$W/cm^2-peak intensity laser pulse interactin with neon atoms. Red dotted line is a fit to the non-adiabatic values.

of chirp towards the wings. The deviation between the two models reach about 10% at the FWHM position.

The ACEP does not simply vary by a factor π from one burst to the next, as could be expected for an infinite driving pulse. At the peak of the pulse, the ACEP is set by the phase and delay of the central harmonic, the variation during the pulse is affected by the variation of the phase and delay with respect to intensity ($\partial \Phi / \partial I$ and $\partial^2 \Phi / \partial q \partial I$).

We observe, that the ACEP and GDD of the individual pulses shift with CEP but follow the same curve, independent of the CEP. Pulse characteristics determined by the envelope of the IR! Cf. [12] where they claim it is a non-adiabatic effect. The actual values are obtained by sampling at the pulse apprearances, which is determined by the electric field zero crossings, i.e. shift with CEP.

We see, that the temporal characterisation of the individual pulses in the attosecond pulse train can be achieved rather accuratelly in the adiabatic model: the main cause for the variation is due to the intensity enve-

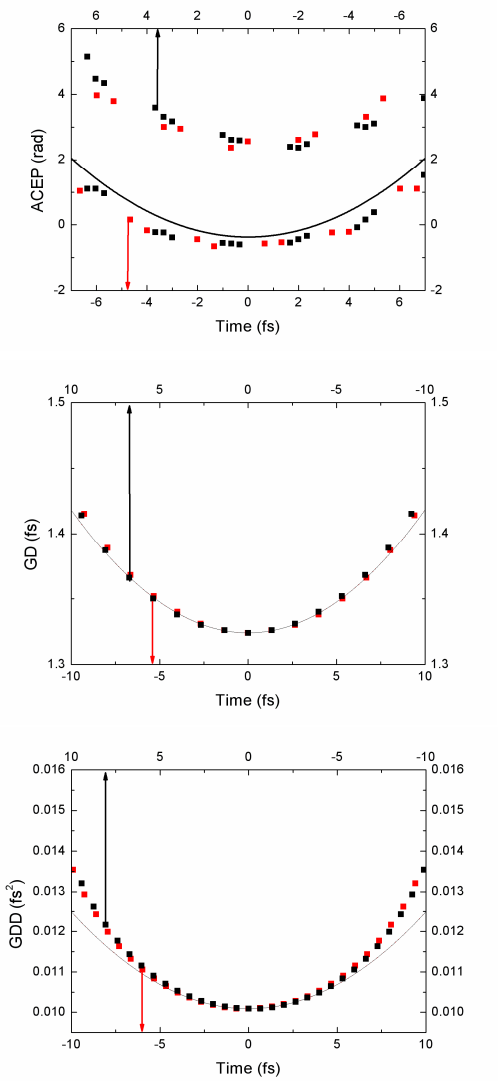

FIG. 5: Pulse characteristics in normal (red symbols, lower axis) and inverted (black symbols, upper axis) time scale for two different fundamental CEP. Solid lines indicate the adiabatic results.

lope of the generating pulse. A true non-adiabtic feature would manifest in the asymmetry of the curve, when not only the instantaneous value of the laser intensity, but the sign of the change or subcycle deviation from a sine curve would play a role. To discover non-adiabatic effects, we plot the pulse characerizing curves in normal and inverted scales in Fig. 5. We notice that the curves are slightly asymmetric, accounting for the non-adiabatic nature.

CONCLUSIONS

In this paper we have studied an attosecond pulse train, generated by a multicycle laser field. We observe pulse-to-pulse variations of ACEP, GD and GDD and connect the variation to the dipole phase derivatives. We calculate the train distortions using both an adiabatic and a non-adiabatic model, and find that there is only a small deviation between the two models.

This research was supported by the Marie Curie European Program (MRTN-CT-2003-505138). KV acknowledges the support of the Magyary Zoltán and NKTH-OTKA Postdoctoral Fellowships.

[1] M. Ferray, *et al.*, J. Phys. B **21**, L31–35 (1988).
[2] P. B. Corkum and F. Krausz, Nature Phys. **3**, 381–387 (2007).
[3] P. Agostini and L. F. DiMauro, Rep. Prog. Phys. **67**, 813–855 (2004).
[4] K. Varjú *et al.*, Phys. Rev. Lett. **95**, 243901 (2005).
[5] J. Mauritsson *et al.*, Phys. Rev. A **70**, 021801(R) (2004).
[6] F. Quéré, Y. Mairesse and I. Itatani, J. Mod. Opt. **52**, 339 (2005).
[7] J. Mauritsson *et al.*, J. Phys. B: At. Mol. Opt. Phys. **38** 2265 (2005).
[8] K. Varjú *et al.*, J. Mod. Opt. **52**, 379 (2005).
[9] M. Lewenstein, *et al.*, PRA **49**, 2117 (1994).
[10] M. Lewenstein, *et al.*, PRA **52**, 4747 (1995).
[11] G. Sansone, *et al.*, PRA **70**, 013411 (2004).
[12] G. Sansone *et al.*, Phys. Rev. Lett. **94**, 193903 (2005).

Attosecond Pulse Generation in Noble Gases in the Presence of Extreme High Intensity THz Pulses

K. Varjú[1], J. A. Fülöp[2], P. Dombi[3], G. Farkas[3], J. Hebling[2]
1-Department of Optics and Quantum Electronics, University of Szeged, 6720 Szeged,Dóm tér 9. Hungary
2-Department of Experimental Physics, University of Pécs, 7624 Pécs, Ifjúság u. 6. Hungary
3-Research Institute for Solid-State Physics and Optics, 1121 Budapest, Konkoly-Thege M. út 29-33, Hungary

varju@physx.u-szeged.hu

Abstract: High harmonic generation by a strong laser pulse in the presence of a THz pulse is simulated. Consequent spectral extension for different laser wavelengths, and the temporal chirp of the synthesized attosecond pulses are studied.

OCIS codes: 190.4180 Multiphoton processes; 320.7110 Ultrafast nonlinear optics

1. Introduction

The shortest – attosecond – light pulses available today are produced by high harmonic generation (HHG) of near-infrared (NIR) laser pulses in noble gas jets [1,2], providing a broad spectral plateau of XUV radiation ending in a cutoff. The minimum pulse duration is determined by the achievable bandwidth (i.e. the position of the cutoff), and the chirp of the produced pulses.

The extension of the cutoff by increasing the laser intensity is limited by the depletion and phase matching problems of the medium. An alternative method demonstrated to produce higher harmonic orders is by using longer pump pulse wavelength, with the disadvantage of decreased efficiency [2].

In a recent theoretical paper [3] it was shown that application of a quasi-DC high strength electric field results in an increase of more than a factor of two in the order of efficiently generated high harmonics. Using the pulses of a CO_2 laser was suggested for the creation of the quasi-DC high strength electric field. However, it is technically very challenging to synchronize these pulses, and the possibility of achieving the needed –a few hundreds of MV/cm– quasi-DC electric field strength is also very questionable.

Alternatively, synchronous production of THz pulses with the IR laser pulse offers a more promising route to exploit the mechanism proposed by [3], leading to both an increased efficiency and a longer plateau of high order harmonics with the promise of even shorter attosecond pulses. The first numerical test of this idea has been reported in [4].

In this contribution we further investigate the method for realistic THz field strengths and short driving pulses, exploring the effect of longer pump laser wavelength on the process. We assume the presence of high intensity THz pulses for supplying the high-strength quasi-DC electric field. Recently the generation of 100 MV/cm focused electric field 55 THz pulses were reported [5].

We calculate the spectrum as well as the chirp of the produced radiation.

2. Method of investigation

We use a non-adiabatic saddlepoint method to determine the generated radiation, following the method of [6]. A generating laser pulse of form

$$E(t) = E_{IR}\sin(\omega_{IR}t)\cos^2\left(\frac{t}{\tau}\right) + E_{THz}\sin(\omega_{THz}t) \qquad (1)$$

has been used, where τ is related to the FWHM duration of the driving pulse T through $\cos(T/2\tau) = 2^{-1/4}$.

We simulate harmonic generation in He atoms, with NIR pulses of peak intensity of 2×10^{14} W/cm^2 (388 MV/cm) and wavelengths 800 nm and 1560 nm. The THz field strength is varied from 0 to 40 MV/cm (the highest field strength currently available).

The generated spectra is calculated for each half-cycle, and coherently summed.

3. Influence of the presence of THz field on the high-harmonic spectrum

As a result of the presence of the THz field, the half-cycle periodicity of the HHG process is broken, leading to the appearance of both odd and even harmonics (see Fig.1a). Furthermore, the addition of a quasi-DC field to the sinusoidal laser field increases the electric field magnitude in one half-cycle, and reduces it in the next half-cycle, thus leading to the generation of radiation with a spectrum split to two plateaus. The two cutoffs are set by the

radiation produced in the consecutive half-cycles. The higher cutoff increases, whereas the lower cutoff decreases with increasing THz field strength (Fig.1b). We also observe, that the relative increase in harmonic order is larger for the longer NIR wavelength.

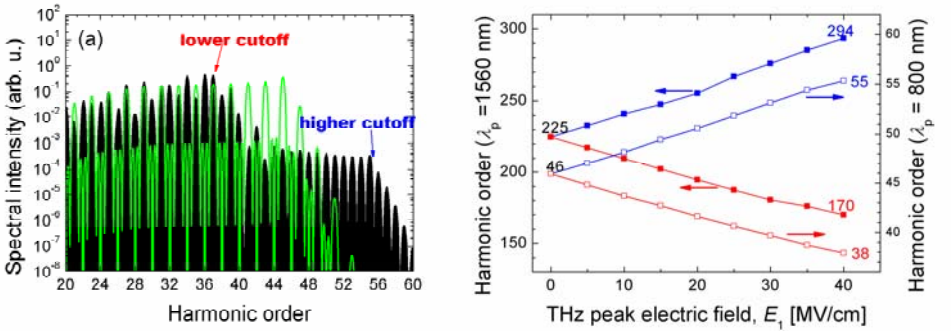

Fig.1. (a) Spectrum of high harmonic radiation produced without (green) and with (black) the THz field for 800 nm laser pulse. (b) Positions of the two cutoffs (higher cutoff: blue symbols, lower cutoffs: red symbols) for two fundamental wavelengths (open symbols: λ=800 nm, filled symbols: λ=1560 nm), as a function of the THz field strength.

4. Temporal characterization of the attosecond pulses.

The broad spectrum of the produced radiation would support the synthesis of attosecond pulses in the absence of a strong chirp. We find, however, in contrast to [4] that the attosecond pulses produced in this scheme are chirped.

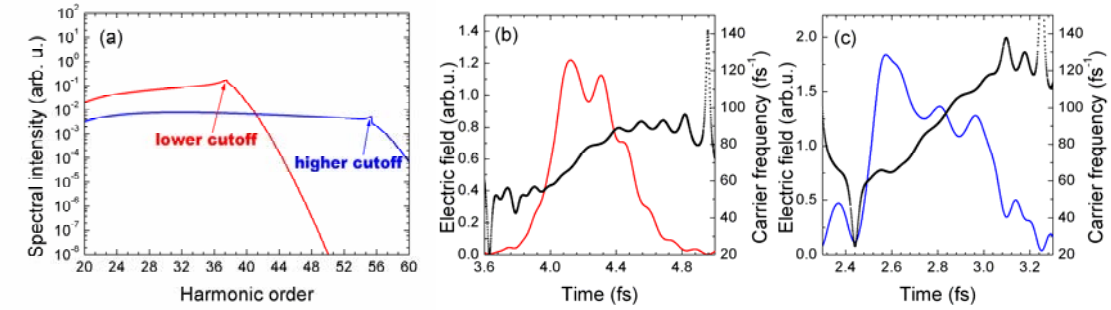

Fig.2. (a) Spectrum of high harmonic radiation produced in two consecutive half-cycles (red and blue curves). (b) and (c) Corresponding attosecond pulses, and their carrier frequencies. The slope of the carrier frequency curve corresponds to the chirp.

The method presented here allows for the production of a broader spectral range of harmonics, leading to the synthesis of even shorter attosecond pulses with suitable chirp compensation techniques.

5. References

[1] Gy. Farkas and Cs. Toth, Phys. Lett. A **168**, 447 (1992).
[2] F. Krausz and M. Yu. Ivanov, Rev. Mod. Phys. **81**, 163 (2009).
[3] Y. Xiang, Y. Niu, S. Gong, Physical Review A **79**, 053419 (2009).
[4] W. Hong, P. Lu, P. Lan, Q. Zhang, X. Wang, Optics Express **17**, 5139 (2009)
[5] A. Sell, A. Leitenstorfer, and R. Huber, Optics Letters **33**, 2767 (2008).
[6] G. Sansone, C. Vozzi, S. Stagira, and M. Nisoli, Phys. Rev. A **70**, 013411 (2004)